RIGA TECHNICAL UNIVERSITY
Faculty of Mechanical Engineering, Transport and Aeronautics
Institute of Mechanics and Mechanical Engineering

Shravan Koundinya Vutukuru
Doctoral Student of the Study Programme "Engineering Technology, Mechanics and Mechanical Engineering"

INTERACTION ANALYSIS OF SIMPLE FORM OBJECTS WITH FLUID AND CONTROL OPTIMIZATION

Summary of the Doctoral Thesis

Scientific Supervisors:

Professor Dr. sc. ing.
IGORS TIPĀNS

Professor Dr. habil. sc. ing.
JĀNIS VĪBA

RTU Press
Riga 2021

Vutukuru, S. K. Interaction Analysis of Simple Form Objects with Fluid and Control Optimization. Summary of the Doctoral Thesis. Riga: RTU Press, 2021. 41 p.

Published in accordance with the decision of the Promotion Council “P-04” of 13 May 2021, Minutes No. 45.

The Doctoral Thesis was developed with the financial support of the Doctoral Research grant of RTU and Faculty of Mechanical Engineering, Transport and Aeronautics.

https://doi.org/10.7250/9789934226656
ISBN 978-9934-22-665-6 (pdf)

DOCTORAL THESIS PROPOSED TO RIGA TECHNICAL UNIVERSITY FOR THE PROMOTION TO THE SCIENTIFIC DEGREE OF DOCTOR OF SCIENCE

To be granted the scientific degree of Doctor of Science (Ph. D.), the present Doctoral Thesis has been submitted for the defence at the open meeting of RTU Promotion Council at on 17 September 2021 14.30 at the Faculty of Mechanical Engineering, Transport and Aeronautics of Riga Technical University, 6B Kipsalas Street, Room 521.

OFFICIAL REVIEWERS

Professor Emeritus Dr. sc. ing. Alģimantas Bubulis
Kaunas University of Technology, Lithuania

Professor emeritus Dr. sc. ing. Ēriks Kronbergs
Latvia University of Life Sciences and Technologies, Latvia

Assistant Dr. sc. ing. Marina Čerpinska
Riga Technical University, Latvia

DECLARATION OF ACADEMIC INTEGRITY

I hereby declare that the Doctoral Thesis submitted for the review to Riga Technical University for the promotion to the scientific degree of Doctor of Science (Ph. D.) is my own. I confirm that this Doctoral Thesis had not been submitted to any other university for the promotion to a scientific degree.

Shravan Koundinya Vutukuru ……………………………. (signature)

Date: ………………………

The Doctoral Thesis has been written in English. It consists of Introduction; 6 chapters; Conclusions; 136 figures; the total number of pages is 112. The Bibliography contains 70 titles.

CONTENTS

GENERAL OVERVIEW OF THE THESIS

Topicality

The rigid body and fluid flow interaction is a very important phenomenon that needs to be explored because of its wide occurence in nature and for its high demand in understanding various engineering and medical applications. One of the best use of this fluid-rigid body interaction phenomenon is to investigate the possiblility of obtaining the energy from the surrounding medium (air, water) when the object is immersed in the fluid. Broadly, there are three main possibilities of interactions with the fluid: (a) stationary rigid body-fluid interaction (still fluid), (b) stationary rigid body in a fluid flow, (c) non-stationary rigid body in a fluid flow.

This completed work of the author and his colleagues covers the following areas that are directly related to the concept or phenomenon of fluid structure interaction: (a) approximate analytical method for fluid-stationary rigid body interaction phenomenon that is of importance to understand non-stationary body motion in fluid flow, (b) interaction analysis of simple form objects, (c) parametric and control optimization of fluid-rigid body interaction problem, (d) synthesis of new devices for energy scavenging through motion modelling of simple form objects and their interaction phenomenon, (e) experiments pertaining to simple form objects subjected to fluid (air)flow. The actual work is carried in two fields: to investigate non-stationary body motion in fluid by analyzing stationary rigid body interaction phenomenon and to extend the interaction phenomenon of non-stationary body motion by simple form objects for the synthesis of new energy scavenging systems and for the tasks of parametric and control optimization of bodies in fluid flow. The terms ‘energy extraction’ or ‘energy scavenging’ refer to the activity that is related to the generation of energy which is the ‘green or clean energy’.

The Aim and Main Tasks of the Work

The main focus of the present work is to investigate in detail the stationary rigid body-fluid (air) interaction phenomenon and to extend the interaction concept for non-stationary body-fluid interaction without requiring ‘space-time’ programming techniques and also the application of the interaction phenomenon in performing engineering tasks of energy scavenging, synthesis of new devices through control and parametric optimization. A simple and straightforward mathematical model is proposed (according to the classical laws of mechanics) that is based on fluid-rigid body interaction phenomenon for simple form objects. The interaction is in detail analysed by using ANSYS software in a uniform flow at low speeds, and then the space around this interaction is split into zones. The task of optimization is considered (in terms of perturbation in parameters and for area control). All calculations and experiments are performed for prevailing wind conditions in Latvia (at 10 m/s).

The research carried out in the work is summarized in the following main directions as a thematically merged set of scientific publications:

1. **New approach for fluid-rigid body interaction phenomenon**
   - A simplified theory for studying the rigid body interaction phenomenon is proposed by the theory of superposition when the body is subjected to a fluid flow.
   - Interaction analysis is carried out for objects in different fluid flow conditions (windless, stationary and non-stationary motion).
   - A mathematical interaction model was proposed to understand the interaction phenomenon.
2. **Interaction of simple form objects**
   - Simple form objects like diamond, square, perforated plate and star prism interaction analysis in fluid flow (air) were carried out and verified through computer programms using ANSYS.
   - A simple and straightforward mathematical model is proposed by studying the interaction phenomenon for convex and concave broken side prisms.
   - ANSYS results are discussed and the new theory is validated.
3. **Approximation for interaction phenomenon**
   - Interaction analysis of simple form objects like flat plate, diamond, perforated plate and star prisms (all stationary) at steady flow of 10 m/s, pressure plots of star prism and error estimation for calculating co-efficient of interaction *C* for the simple form objects (diamond, flat plate and perforated plate).
   - Interaction phenomenon extended for the investigation of concave and convex broken side prisms immersed in fluid flow.
   - Concept of diving and flying objects is analysed.
   - ANSYS simulation results are provided.
4. **Parametric and control optimization for interaction phenomenon**
   - Onboard energy scavenging task using simple form object like flat plate, perforated plate as a model for flapping/oscillating robotic fish tail is analysed through the parametric optimization.
   - Damping due to impact and due to harmonic excitation from fluid and structure interaction are analysed and explained.
   - Control optimization for robotic fish movement (horizontal, vertical) with force and control action is analysed.
5. **Synthesis of new energy scavenging systems**
   - Efficent and innovative energy scavenging systems of 1D.O.F, 2D.O.F and 3D.O.F are analysed and the process and results of theoretical interaction models are dicussed and explained.
6. **Experiments**
   - Experiments to validate the theory using simple pendulum in still air are performed.
   - A new flapping/oscillating device is investigated.
   - Innovative patented application for the purpose of energy scavenging from fluid flow by a flat plate is mentioned.

Research Objective

In the current work, the main objective of the research is to study the interaction of fluid with a stationary rigid body in the fluid flow and to extend the concept (through the post-processing results of the steady state case of the stationary body in fluid) for non-stationary motion of the object when immersed in the fluid medium (air or water). Newtonian mechanics is applied considering the velocities of vectors in different directions. This concept of mathematical modelling through **approximate** differential equations of motion can be solved numerically through integration that helps overcome the complicated task of 'space-time' programming techniques for solution of simple engineering issues.

The theory/concept of non-stationary motion in fluid medium is further extended to obtain or scavenge energy from fluid-body interaction and in the synthesis of new systems or to analyze the diving or flying objects in fluid flow.

Research Hypotheses

The main hypotheses of the work are based on the basic hypotheses of Newtonian mechanics:

1) superposition principle equation of motion for the particle system in the fluid medium (differential form);
2) rigid body and fluid particles impact in the windward side (pressure zone), pressure at the leeward side (suction zone) is created by the fluid particles;
3) viscosity of the fluid medium is ignored;
4) the fluid is assumed to be incompressible (density is constant);
5) in the pressure zone, the vector of the absolute velocity of the fluid flow V_0 is the same at all contact points of the object.

All the above hypotheses have been analyzed through numerical simulations and experiments performed using wind tunnel as well as the movement of the pendulum in the open air. As a result, a new and a better approximate scientific theory was developed. The new theory differs from all the existing theories in that it is not always necessary to perform a 'space-time' analysis of non-stationary rigid-body fluid interactions. The interaction phenomenon of non-stationary rigid body and fluid flow interaction could be well understood through a stationary rigid body and fluid flow interaction phenomenon, which means there is no need to perform extensive 'space-time' programming techniques for simple engineering tasks.

Research Novelty

1. Comercially available software for computational fluid dynamics study with 'space-time' programming techniques involves constant re-meshing for geometries in non-stationary motion when subjected to fluid flow and, additionally, are computationally very expensive and at the same time they offer approximate solution at the end. It is therefore important to look for an alternative approach that helps to perform simple

engineering tasks related to non-stationary rigid body motion in a fluid medium (air or water) without requiring labour intensive 'space time' programming techniques.
2. The proposed method (theory) and methodologies in the work suggest the use of classsical mechanical methods for understanding the physics of non-stationary rigid body-fluid interaction in a continuous medium (air or water) ignoring the viscosity of the fluid medium and thereby it is possible to obtain dissipated forces through reduction of their principal vectors and principal moments at the centre of mass of the rigid object (system). The obtained corresponding equivalent relations allow forming differential equations of body motion, which are numerically integrated accordingly. Upon integration, it is possible to perform parametric optimization with a computer and synthesize new efficient systems for efficient use of energy during fluid movement or to create new 'green energy' systems for fluid flow around a rigid body object or to realise a flying or diving object in a fluid medium.

Practical Application of the Thesis

1. The theory and methodology for the interaction of objects with fluid for different cases (stationary object, still fluid, and non-stationary object in a flowing fluid) can be used in the systhesis of new 'clean energy' devices and also for the design of flying and diving robots/machines.
2. The results of computer modelling for 2D and 3D are helpful to solve the task of form optimization.
3. Control of robotic fish tail actuator (single or dual) can be used for energy restoration (to recharge on-board power pack).
4. A patent application under the title "Wind energy conversion device" has been developed and submitted that is based on the fluid-rigid body interaction principle with a linear generator.

Thesis Approbation and Publications

Scientific articles indexed in Scopus and/or Web of Science database

1. Tipans I., Viba J., Irbe M., Vutukuru S. K. 2020. Investigation of dual varying area flapping actuator of a robotic fish with energy recovery. *Agron. Res.* 18, 1046–55.
2. Tipans I., Viba J., Irbe M., Vutukuru S. K. 2019. Analysis of non-stationary flow interaction with simple form objects. *Agron. Res.* 17, 1227–34.

Full-text conference papers published in conference proceedings indexed in Scopus and/or Web of Science database

3. Vutukuru S. K., Tipans I., Viba J., Irbe M. 2020. Form optimization and interaction analysis of plane symmetry prism in air. *Engineering for Rural Development.* vol. 19, pp. 739–46.

4. Spade K., Vaicis I., Vutukuru S. K., Irbe M. 2020. Analysis of granule layer impact interaction on vibrating 2D prism. *Engineering for Rural Development.* vol. 19, pp. 1463–9.
5. Vutukuru S., Viba J., Tipans I., Viksne I., Irbe M. 2019. Analysis of flat plate vibrations by varying frontal area to the flow. *Engineering for Rural Development.* vol. 18, pp. 1408–14.
6. Tipans I., Viba J., Vutukuru S. K., Irbe M. 2019. Vibration analysis of perforated plate in non-stationary motion. *Vibroengineering Procedia.* vol. 25, pp. 48–53.
7. Tipans I., Viba J., Vutukuru S. K., Irbe M. 2021.Varying area vibrating structure in a fluid for energy gain. *Advances in Systems Engineering. Lecture Notes in Mechanical Engineering. Springer, Singapore.* pp. 757–770.
8. Tipans I., Viba J., Vutukuru S. K., Irbe M. 2021. Optimization of energy extraction using definite geometry prisms in air. *Latvian Journal of Physics and Technical Sciences*. Vol. 58(2), pp. 19–31.
9. Tipans I., Viba J., Vutukuru S. K., Irbe M. 2021. Action of pendulum in transient fluid flow. *Engineering for Rural Development.* vol. 20, pp. 275–280.
10. Beresnevich V., Vutukuru S.K., Irbe M., Kovals E., Eiduks M., Burbeckis K., Viba J. Wind energy conversion generator. *Engineering for Rural Development.* Vol. 20. pp. 955–960.

Patent application

1. Vēja enerģijas pārveidošanas iekārta (Wind Energy Conversion Device). Submitted on 18.12.2020., LVP2020000092.

Author's Contribution to Publications

All scientific publications have been written in collaboration with supervisors Professor Jānis Vība and Professor Igors Tipāns and co-author and consultant Mārtiņš Irbe in the development of publications. The work on scientific publications was collectively planned and accomplished by the authors. The percentage of research work contributed by the author to scientific publications is summarized in Table 1.

Table 1

Contribution to the Development of Scientific Publications

Publication No.	Activity	Contribution
1.	Experimental equipment design, literature, experiments, data processing, numerical modelling	75 %
2.	Research of literature, simple form object analysis, numerical modelling and graphical representation, 2D & 3D flow simulations	75 %

Continuation of Table 1

3.	Research of literature, design, prototyping, 2D & 3D flow simulation, wind tunnel experiments, data processing and graphical representation, mathematical modelling	75 %
4.	Modelling of granular fraction motion using approximate force determination method for pressure and suction zones	5 %
5.	Rigid body shape geometry optimization analysis of fluid and body interactions, experimental model, experiments in wind tunnel, 2D & 3D simulations	75 %
6.	Analysis, optimization and synthesis of non-stationary fluid and body interaction, wind tunnel experiments, numerical modelling, 3D simulations, experimental model	100 %
7.	Parametric optimization, research literature, numerical modelling, body motion analysis	40 %
8.	Geometry design and research literature	100 %
9.	Experiments, simulation and results analysis	50 %
10.	Literature review, results analysis and mathematical simulation	50 %

Structure of the Thesis and Main Results

The structure of the Thesis is summarized in 6 chapters.

In Chapter 1, the latest advancements and the state of the art in research are reviewed.

In Chapter 2, a new approximate analytical method through a mathematical model for fluid-rigid body interaction is analysed and summarized in scientific publication No. 8, with three main topics covered:

1) fluid-rigid body interaction phenomenon with motionless fluid;
2) stationary rigid body object interaction with air (fluid) at low speeds;
3) moving object in a fluid flow (at low speeds).

Chapter 3 summarizes scientific publications No. 2, 3, 5, and 6 on fluid (air) flow, with the following main topics covered:

1) analysis of simple rigid body-fluid flow interaction phenomenon for steady and unsteady case;
2) interaction phenomenon for flow object interaction (concave and convex side prism).

Chapter 4 summarizes other studies of fluid dynamics in scientific publications No. 2, 3, and 7 with four main topics covered:

1) variable area rigid body structure vibrations in fluid flow for energy extraction; optimization task;
2) variable area rigid body structure model for vibrations in a fluid flow for energy extraction and a mathematical model of the horizontal motion of one tail or dual tail of a fish robot in a fluid;

3) vibration damping of fluid-rigid body interactions at low speeds;
4) control optimization methods (force and area control) for horizontal and vertical motion of the body.

Chapter 5 summarizes other studies of fluid dynamics in scientific publications No. 3, 7, and 10 with the following topic covered:

1) synthesis of new devices for the purpose of energy scavenging.

Chapter 6 summarizes other studies of fluid dynamics in scientific publications No. 3, 5, 6, and 9 with the following main topics covered:

1) experiments related to flat plate;
2) experiments related to perforated plate;
3) validation of the interaction phenomenon theory (mathematical model).

Thesis for Assertion

1. Standard explanations found in the literature on interaction of fluid and rigid body are not accurate: it has been proved that the lowest pressure does not always occur at the visually longest fluid flow line (i.e., as the highest local velocity). In fact, there is a suction phenomenon, which then also reduces pressure and can be realised immediately adjacent to the body at the leeward side.
2. Viscosity may be ignored in engineering calculations for fluid-solid interaction analysis (only for air medium). This is justified because all computer modelling programs (which respect viscosity) are also approximate. Also, considering the interaction phenomenon, the shape of the object, nature of flow (laminar or turbulent) are of primary importance. Viscosity of fluid medium (only for air) is of secondary importance.
3. In the analysis of air-rigid body interactions, the principle of superposition for non-stationary body motion or relative motion in the fluid flow can be applied, i.e., the interaction phenomenon can be divided into two zones: the pressure zone and the suction zone. The laws of classical mechanics including Brownian chaotic motion of particles are to be considered for better analysis.
4. The approximate theory obtained in the description of the interaction between air and a rigid body can be applied to the engineering estimates for the description of interaction between water and solid considering the density and viscous effects.
5. The differential equations of fluid-rigid body interaction obtained in the work can be applied to solve analysis, optimization, and synthesis problems without using complex and time-consuming ‘space-time’ programming approximate methods.

INTRODUCTION

The dissertation as a thematically unified set of scientific publications has been developed by participating in different practical study directions. Based on this, the following work development stages were performed that are summarised in Table 2. The optimization and synthesis task is carried out as mentioned in the book by J. Viba[1].

Table 2

Development Stages of the Dissertation as a Thematically Unified Set of Scientific Publications

Stages	Interaction phenomenon	Fluid (air) flow	Control and parametric optimization
Initial analysis of the problem	+	+	
1. Study of new approach	+	+	
2. Analysis of interaction phenomenon	+	+	
3. Simple form objects and interaction	+	+	
4. Interaction problem	+	+	+
5. Synthesis of new devices	+	+	+
6. Experiments		+	

Chapter 1. Introduction on existing analytical methods and interaction phenomenon applications.

1.1. Applications of interaction priciples.

1.2. Opinions and conclusions.

Chapter 2. New approach and approximate analytical method for fluid-rigid body interaction

2.1. A simplified theory for studying the rigid body interaction phenomenon is proposed by the theory of superposition when the body is subjected to fluid flow.

2.2. Interaction analysis is carried out for objects in different fluid flow conditions (windless, stationary and non-stationary motion).

2.3. A mathematical interaction model was proposed to understand the interaction phenomenon that could help in performing engineering tasks of analysis and optimization of flying and diving objects.

Chapter 3. Interaction analysis of simple form objects

3.1. Simple form objects like diamond, square, perforated plate and star prism interaction analysis in fluid flow (air) were carried out and verified through computer programms using ANSYS.

[1] J. Viba "Optimization and Synthesis of Impact Vibration Machines" (in Russian), "Zinatne" Publishers. 1988, 253 p.

3.2. A simple and straightforward mathematical model is proposed by studying in the interaction phenomenon for convex and concave broken side prisms.
3.3. ANSYS results are discussed and the new theory is validated.
3.4. Concept of diving and flying motion of objects is analysed.

Chapter 4. Parametric and control optimization for fluid-rigid body interaction problem

4.1. Onboard energy scavenging task using simple form object like flat plate, perforated plate as a model for flapping/oscillating fish tail (robotic fish) is analysed through the parametric optimization.
4.2. Vibration damping due to impact and also from harmonic excitation from fluid and structure interaction are analysed and explained.
4.3. Control optimization for robotic fish movement (horizontal, vertical) with force and control action is analysed.

Chapter 5. Synthesis and motion modelling of new energy scavenging systems

5.1 Efficient and innovative energy scavenging systems in 1D.O.F, 2.D.O.F and 3.D.O.F are analysed, and the process and results of the theoretical interaction models are dicussed and explained.

Chapter 6. Experiments

6.1. Simple form objects experiment in wind tunnel.
6.2. New flapping device (patent application).

1. APPLICATION OF NUMERICAL METHODS OF INTERACTION ANALYSIS

The fluid-rigid body interaction analysis is basically performed to predict and mitigate the following interaction phenomenon:

- flutter,
- galloping,
- sloshing,
- Vortex Induced Vibrations (V.I.V).

The above-mentioned interaction application for fluid-structure finds wide demand in the field of aerospace technologies (wing flutter, flow over turbine blades), biomedicine (elastic artery modelling for stent design), automotives (design of heat exchangers), and marine engineering (safe and functional marine structures).

1.1. Further Research on the Topic

The main part of the present work specifically focuses solely on rigid body-fluid (air) interaction, does not consider flow reattachment or flow-separation phenomenon and offers an alternative approach to study the interaction phenomenon and its advantages. The main basic idea of the approach/methodology in the current work is to have a simplified approach for interaction phenomenon through a straightforward mathematical model and not considering the viscous nature of fluid medium (air). Therefore it is an approximate theory for non-stationary body-fluid interactions that considers inputs (post-processing results) from stationary rigid body-fluid interaction model performed in ANSYS fluent where the Steady State RANS equation is solved with the help of k-ε realizable turbulence model. The concept discussed in the work will offer an alternative approach for ‘space-time’ programming techniques and also helps solving the engineering tasks of optimization and synthesis for simple form objects without requiring huge computational efforts.

The novelty of interaction analysis approach for the current research work for fluid-rigid body interaction phenomenon is discussed in detail in the subsequent sections. It is believed that the approach discussed helps to solve simple engineering tasks without requiring time consuming programming techniques.

2. NEW APPROACH FOR FLUID (AIR)-RIGID BODY INTERACTION

In this chapter, three different cases for the fluid-rigid body interaction are investigated: (a) moving body (prism) in low speed or windless air; (b) stationary bodies (prism) in air flow; (c) moving body (prism) in airflow. The physics of rigid body (prism) and air interaction is simplified by using superposition principles, i.e. by taking into account the upstream and downstream rigid body (prism) and fluid interaction phenomenon which was found to vary with change in speed.

2.1. Object Interaction with Still Fluid

The space around rigid body - fluid interaction is investigated, and by considering the very small air element in the pressure zone (Publication No. 8[2]), according to the theorem of change in momentum to analyze the air flow-plate interaction in differential form given by Meriam *et al*.[3] is used and the principle proposed in the present work (superposition principle) taking in the projection of the area normal N_1, before and after collisions for the fluid-body interaction from Brownian interaction to prism (Figs. 2.1 and 2.2) we obtain:

$$\begin{gathered} m_{10}VB_1 - (-m_{10}VB_1) = -N_1\mathrm{d}t, \\ m_{10} = VB_1\mathrm{d}t\mathrm{d}L_1B\rho, \\ p_{10} = \frac{|N_1|}{\mathrm{d}L_1\,B}, \end{gathered} \tag{1}$$

where m_{10} – Brownian interaction mass; VB_1 – an average air normal velocity in pressure zone; N_1 – normal force to small element from air; dt – infinitively small time interval. dL_1 – width of small element; B – prism height, perpendicular to the plane of motion; ρ – density of air; p_{10} – atmospheric pressure in pressure zone. From prism - air interaction at windward side (pressure side):

$$\begin{gathered} m_1v\cos(\beta_1) - 0 = \Delta N_1\mathrm{d}t \\ m_1 = v\cos(\beta_1)\,\mathrm{d}t\mathrm{d}L_1B\rho, \\ \Delta p_1 = \frac{|\Delta N_1|}{\mathrm{d}L_1\,B}, \end{gathered} \tag{2}$$

where m_1 is boundary layer mass due to interaction; v is prism velocity; β_1 is angle between velocity v and normal N_1; ΔN_1 is additional normal force, acting to prism; Δp_1 is pressure increase in pressing zone.

[2] https://www.sciendo.com/article/10.2478/lpts-2021-0009
[3] Meriam J. L., Kraige L. G. and Bolton J. N. Engineering Mechanics: Dynamics. 8th ed. New York: John Wiley& Sons; 2016. 736 p. ISBN: 9781119044819 1119044812.

From the system of six equations (1) and (2), it is possible to find six unknowns. The two unknowns are required to solve the following calculations:

$$p_{10} = 2VB_1{}^2 \rho dt, \tag{3}$$

$$\Delta p_1 = v^2 \rho dt\, (\cos(\beta_1))^2, \tag{4}$$

However, for the suction zone, two hypotheses are proposed. These hypotheses should be tested experimentally or by using numerical computer programs.

The first hypothesis in suction zone pressure reduction Δp_{21} over the entire surface is constant and proportional to the square of velocity v:

$$\Delta p_{21} = -\rho C_1 v^2, \tag{5}$$

$$p_{20} = 2VB_2{}^2 \rho dt, \tag{6}$$

where C_1 is constant; and VB_2 is average air normal velocity (suction zone).

The second hypothesis. In suction zone pressure reduction Δp_{22} over the entire surface is not constant and proportional to the square of the velocity v, and depends on the normal N_2 to the surface, angle β_2:

$$\Delta p_{22} = -v^2 \rho C_2 \cos(\beta_2), \tag{7}$$

$$p_{20} = 2VB_2{}^2 \rho dt, \tag{8}$$

where C_2 is a constant.

The differential relations (3)–(8) can be used in engineering analysis at low speeds. For practical engineering calculations $VB_1 = VB_2$ for low velocity $v \ll VB_1$ and $v \ll VB_2$ ranges. Then $p_{01} = p_{02} = p_0$, where p_0 is the mean atmospheric pressure around the prism. Interaction phenomenon could be understood for stationary body (in air) or for rectilinear translation motion of prism (in air) considering the relative motion in (3)–(8).

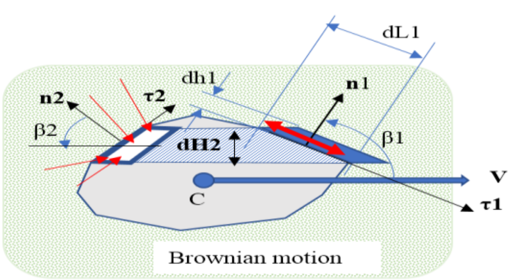

Fig. 2.1. Rectilinear translation (non-rotating) motion body in windless air.

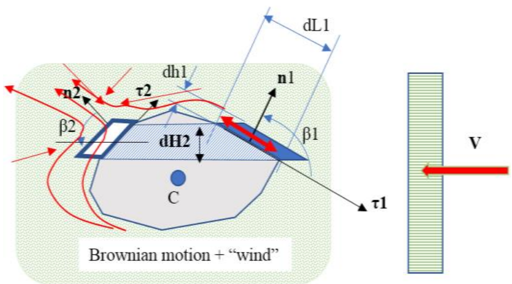

Fig. 2.2. Model of air interactions with stationary prism.

2.2. Stationary Rigid Body (Flat Plate) in Air at Low Speeds

Interaction phenomenon for fluid-rigid body interaction in the case of simple flat plate geometry to obtain the mathematical modelling is explained in Fig. 2.3. The theorem of the change in momentum at the upstream (the pressure side) of flow expressed in differential form is given by (9) and (10).

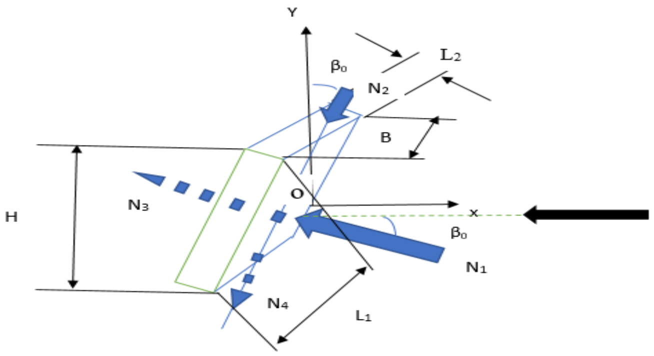

Fig. 2.3. Model in the case of flat plate.
L_1, B – length of flat plate sides; L_2 – thickness of plate; A_1, A_2 – area of sides;
N_1, N_2 – centre forces of additional pressure in frontal sides; N_3, N_4 – centre forces of vacuum (thin) side; V – flow velocity from right to left.

$$\mathrm{d}m \cdot v \cos(\beta_{\mathrm{fp}}) = \mathrm{d}N\mathrm{d}t, \tag{9}$$

$$\mathrm{d}m = v \cos(\beta_{\mathrm{fp}})\, \mathrm{d}L\mathrm{d}tB\rho, \tag{10}$$

where dm – mass of the elemental volume of the flow stream velocity v; β_{fp} – the angle between the flow and the surface at the normal point of impact (for flat plate); dN – the impact force in the direction of the normal surface of the elemental area; t – time; dL – the elemental length of the surface; B – width of the object, ρ – density of air (fluid).

Integrating (9) and (10) additional pressure and forces N_1, N_2 perpendicular to both sides (11) and (12) are obtained (Publication No. 5[4]).

$$N_1 = A_1 v^2 \rho \left[\cos(\beta_{\mathrm{fp}})\right]^2, \tag{11}$$

$$N_2 = A_2 v^2 \rho \left[\sin(\beta_{\mathrm{fp}})\right]^2, \tag{12}$$

where A_1, A_2 – area of sides on the pressure and suction sides, respectively.

At the suction-vacuum (downstream) along the edge of the body it is realized that there exists constant pressure as shown in Fig. 3.4 proportional to density ρ multiplied by the flow velocity square as represented in (13) and (14).

$$N_3 = A_1 v^2 \rho C, \tag{13}$$

$$N_4 = A_2 v^2 \rho C, \tag{14}$$

where C is a constant depending on the form and speed of the incomming flow, for subsonic case $0 < C < 1$.

From the centre of plate O, there arise two components of interaction forces along the flow and in perpendicular to the flow given by (15) and (16), respectively.

$$f_x = -HB\rho v^2 \left[C + \frac{\cos(\beta_{\mathrm{fp}})^3 + d\sin(\beta_{\mathrm{fp}})^3}{\cos(\beta_{\mathrm{fp}}) + d\sin(\beta_{\mathrm{fp}})}\right]. \tag{15}$$

[4] http://www.tf.llu.lv/conference/proceedings2019/Papers/N147.pdf

$$f_y = L_1 B \rho v^2 \left(C \left[\sin\left(\beta_{\mathrm{fp}}\right) - d\cos\left(\beta_{\mathrm{fp}}\right) \right] \right) + \sin\left(\beta_{\mathrm{fp}}\right) \left[\cos\left(\beta_{\mathrm{fp}}\right) \right]^2 + d\left[\cos\left(\beta_{\mathrm{fp}}\right) \right]^3. \quad (16)$$

Also, from Fig. 2.3:

$$H = L_1 \left[\cos\left(\beta_{\mathrm{fp}}\right) + d\sin\left(\beta_{\mathrm{fp}}\right) \right];\ d = \frac{L_2}{L_1}, \quad (17)$$

where d is the ratio of edges L_2/L_1; f_x is the direction of x axis force component, named in fluid dynamics as drag force; f_y is parallel to y axis force component, named in fluid dynamics as lifting force; H is section height perpendicular to flow.

2.3. Moving Object in a Running Fluid

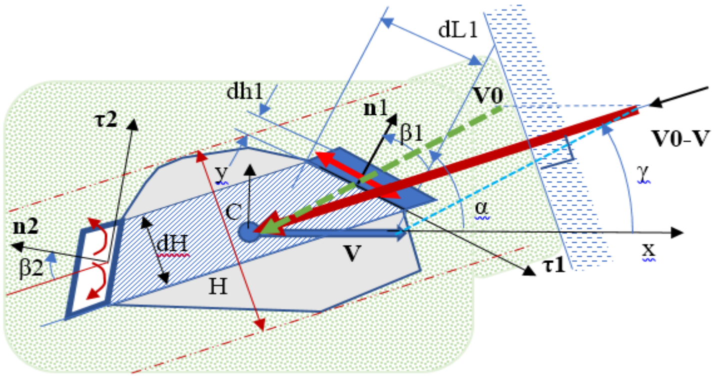

Fig. 2.4. Model of moving prism in airflow.

Interaction of a moving prism in a moving air stream is shown in Fig. 2.4. Angle γ from the elementary parallelograms with normal directions N_1 and N_2, from vectors V and V_0 on the x and y-axes, we obtain (18) and (19).

$$V_{\mathrm{r}} = \sqrt{[-V_0\cos(\alpha) - V]^2 + [-V_0\sin(\alpha)]^2}. \quad (18)$$

$$\cos(\gamma) = \frac{-V_0\cos(\alpha) - V}{\sqrt{[-V_0\cos(\alpha) - V]^2 + [-V_0\sin(\alpha)]^2}}. \quad (19)$$

where V_{r} is relative velocity; V_0 is wind velocity as vector; V is prism rectilinear translation motion velocity as vector; and α is a V_0 flow angle.

3. APPROXIMATION FOR INTERACTION PHENOMENON

ANSYS fluent software was used to carry out the numerical simulations. The steady state RANS (Reynolds Averaged Navier Stokes) equation is solved using k-ε realizable turbulence model for a constant speed of 10 m/s keeping in view the prevailing wind and weather conditions in Riga, Latvia. The length and depth of all the forms are taken to be 0.16 m.

From the results of numerical simulations, it is now realized that the region around the fluid-body interaction can be split into two zones. In the upstream side there exists a pressure zone and in the downstream side just behind the body there is a suction or vacuum zone (leeward side) Fig. 3.2. The value of interaction constant C from (15) and (16) has to be calculated by using the numerical techniques or experiments. It was found that the value of C (interaction constant) is positive and less than 1 (at low speeds).

3.1. 3D Diamond Prism

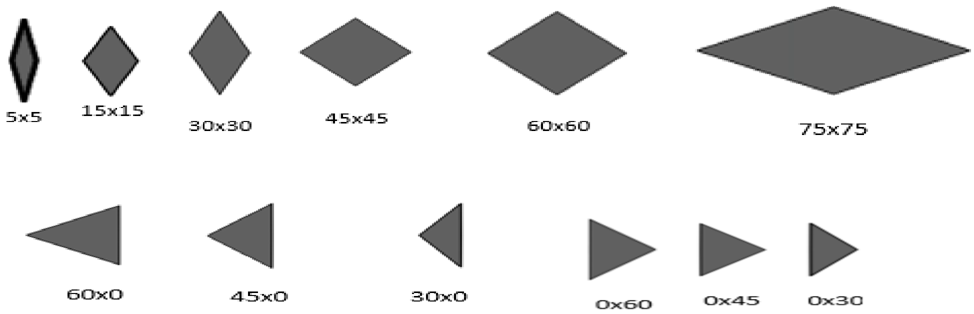

Fig. 3.1. All prism shapes.

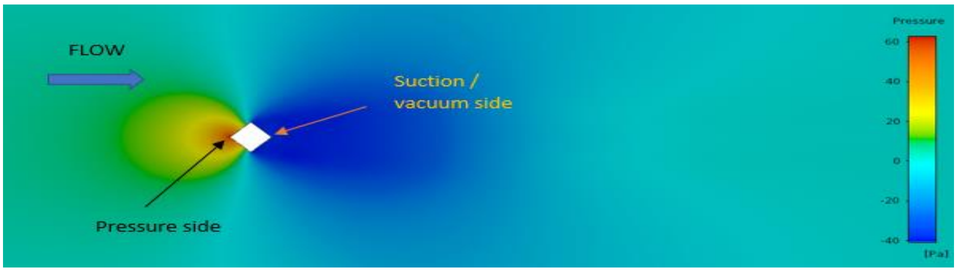

Fig. 3.2. Concept of zones for a diamond (45 × 45) prism at constant speed of 10 m/s.

Since the interaction force (drag force) is a fluctuating, non-constant in 2D analysis, an average interaction force is considered.

Similar to the mathematical model developed earlier for the flat plate, the same concept is extended for diamond form, for the diamond shaped rigid body f_{xd}, along the direction of flow is given by (20).

$$f_{x\mathrm{d}} = -HBv^2\rho[C + \cos(\beta_\mathrm{d})^2]\,, \tag{20}$$

where B – body width; H – section height, perpendicular to the flow; β_d – the angle between the flow and the surface at the normal point of impact; ρ – density of the fluid; D – theoretical interaction force along flow (21); D_{ex} – calculated interaction force along flow (21); and approximated D_p – interaction force as the fifth-degree polynomial function (22):

$$D = C + \cos(\beta_d)^2\,; \tag{21}$$

$$D_{ex} = \frac{f_{xde}}{Av^2\rho}, \tag{22}$$

$$D_p(\beta_d) = 1.5 + 3.7266{\beta_d}^3 - 1.5249{\beta_d}^4 - 0.101\,35{\beta_d}^5 - 2.8129{\beta_d}^2 + 0.2823\beta_d, \tag{23}$$

where f_{xde} is interaction force for diamond plate along the flow direction. From equations (21) and (23) it follows that $C = 0.5$ when $\beta_d = 0$. Therefore, the following approximation formula is recommended for interaction coefficient in the case of diamond shaped body:

$$D = 0.5 + [\cos(\beta_d)]^2 \tag{24}$$

The estimation of the accuracy of the approximate formula (24) for diamond-shaped object at $C = 0.5$ is analysed and the difference is less than 5 % (percentage average value).

3.2. Fluid-Body Interaction Analysis of Star Prism and Flat Plate

Interaction analysis for a star prism where the steady state RANS equation is solved at a speed of 10 m/s is shown in Fig. 3.3, and pressure distribution is shown for steady and unsteady case in Fig. 3.4. The suction or vacuum zone is realized and in this zone the pressure is almost constant along the length and only varies with speed (publication No. 2[5]), nature of flow (steady or unsteady) and form is dependent at the edges as shown in Fig. 3.4. In the case of flat plate, 2D numerical simulations for flat plate are investigated for coefficient C. By varying β_{2d}, only the mean values of interactions are analyzed and part of interaction $D_1(\beta_{2d})$ is given by (25):

$$\begin{aligned} D_1(\beta_{2d}) = {} & -0.101\,353\,259\,849\,2(\beta_{2d})^5 - 1.524\,924\,115\,636\,690\,045\,8(\beta_{2d})^4 \\ & + 3.726\,620\,425\,6(\beta_{2d})^3 - 2.812\,935\,237\,499\,053\,63(\beta_{2d})^2 \\ & + 0.282\,306\,1\beta_{2d} + 1.5. \end{aligned} \tag{25}$$

The mean value of the percentage error is found to be less than 5 %.

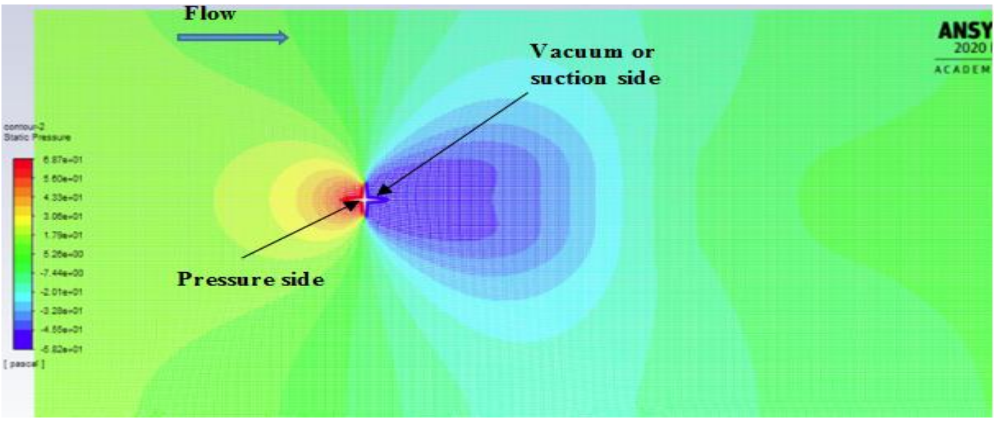

Fig. 3.3. Static pressure contour over stationary star prism at a constant speed of 10 m/s.

[5] https://dspace.emu.ee/xmlui/handle/10492/4796

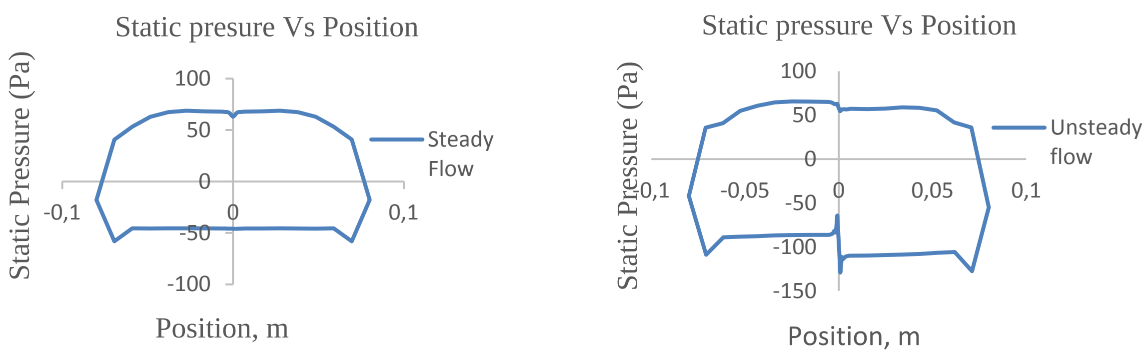

(a) (b)

Fig. 3.4. Static pressure plot for stationary star prism for (a) steady flow, (b) unsteady flow at constant speed of 10 m/s.

For 3D square flat plate, (15) is taken, multiplying by a factor of 0.5 as in (26).

$$f_x = \frac{Av^2\rho}{2}\left[C + \frac{\cos(\beta_{3d})^3 + d\sin(\beta_{3d})^3}{\cos(\beta_{3d}) + d\sin(\beta_{3d})}\right] \tag{26}$$

where A is area of the body subjected to fluid flow (wetted area). For the computation result the interaction force is estimated to be in terms of β_{3d}:

$$\begin{gathered} D_3(\beta_{3d}) = -8\cdot 10^{-12}\beta_{3d}{}^5 + 2\cdot 10^{-8}\beta_{3d}{}^4 + 2\cdot 10^{-7}\beta_{3d}{}^3 \\ -0.0004\beta_{3d}{}^2 - 0.0013\beta_{3d} + 2.0463. \end{gathered} \tag{27}$$

Similarly, for drag force experiments at 10 m/s, the results when approximated in the form of a curve, 5th degree polynomial, resulted in equation (28):

$$\begin{gathered} D_{e3}(\beta_{e3d}) = 10^{-11}\beta_{e3d}{}^5 + 2\cdot 10^{-8}\beta_{e3d} + 10^{-7}\beta_{e3d} \\ -0.004\beta_{e3d}{}^2 - 0.0016\,\beta_{e3d} + 2.1796. \end{gathered} \tag{28}$$

From (26), calculating the drag force for the given geometry, the value of constant $C = 0.31$ is obtained for $\beta_{e3d} = 0°$. Thereby, for plate in 3D at $\beta_{e3d} = 0°$ is taken as 1.31. It was observed that the maximum error measured at $\beta = 0°$ ($\beta_{e3d} = 0°$ and $\beta_{3d} = 0°$) in computations and experiments was ~6 % as analysed.

3.3. 3D Perforated Plate Interaction Analysis

The total area of perforations was maintained at half the area of the flat plate. The drag was also reduced with the perforated plate as compared to the simple flat plate. There was no presence of recirculating streamlines downstream. The interaction force for the perforated plate is given by (Publication No. 6[6]):

$$If_x = -kBHv^2\rho\left[C + \frac{\cos(\beta_p)^3 + d\sin(\beta_p)^3}{\cos(\beta_p) + d\sin(\beta_p)}\right]. \tag{29}$$

[6] https://www.jvejournals.com/article/20801

3.4. Flow and Object Interaction (Convex and Concave Form)

3.4.1. Convex Broken Side Prism Model Immersed in Fluid Flow-Investigation

The four-corner prism with convex broken side is shown in Fig. 3.20. The force can be calculated through pressure on the sides by applying the change in momentum principle (30) along the flow direction and (31) along the perpendicular direction (Publication No. 3[7]).

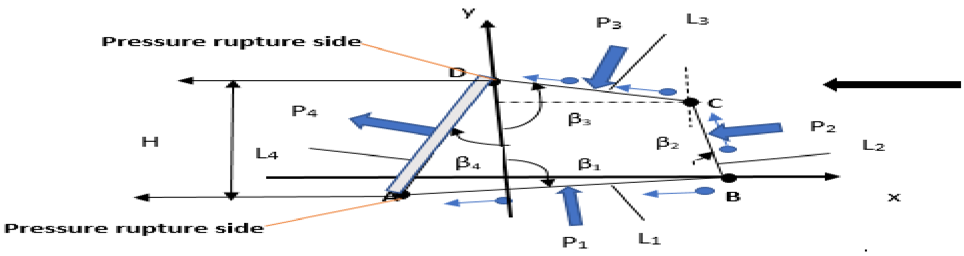

Fig. 3.5. Model for convex prism.
L_1, L_2 – length of sides; β₁, β₂ – frontal angles; H – height of prism;  – symbol of flow direction on the body surface as a result of air-body interaction.

$$-f_x = V^2 B\rho\{L_1[\cos(\beta_1)^3] + L_2[\cos(\beta_2)^3] + L_3[\cos(\beta_3)^3 - C_{12}C_{23}\cos(\beta_2)\cos(\beta_3)\sin(\beta_3 - \beta_2)] + L_4 C_4 \cos(\beta_4)\}; \tag{30}$$

$$-f_y = V^2 B\rho\{L_1[\cos(\beta_1)^2]\sin(\beta_1) + L_2[\cos(\beta_2)]^2\sin(\beta_2) + L_3[\cos(\beta_3)^2\sin(\beta_3) - C_{12}C_{23}\cos(\beta_2)\sin(\beta_3)\sin(\beta_3 - \beta_2)] + L_4 C_4 \sin(\beta_4)]\}. \tag{31}$$

3.4.2. Analytical Investigation for Concave Broken Side Prism

For concave side, there exists the impact force N_3 on the edge of the inner breakage, as shown in Fig. 3.6, given by (32):

$$N_3 = L_2 B\rho V^2 \cos(\beta_2)\sin(\beta_2 - \beta_3)\,[0.5 + 0.5\sin(\beta_2 - \beta_3)]. \tag{32}$$

Here the criterion for taking the concave case is when $\sin(\beta_2 - \beta_3) \geq 0$.

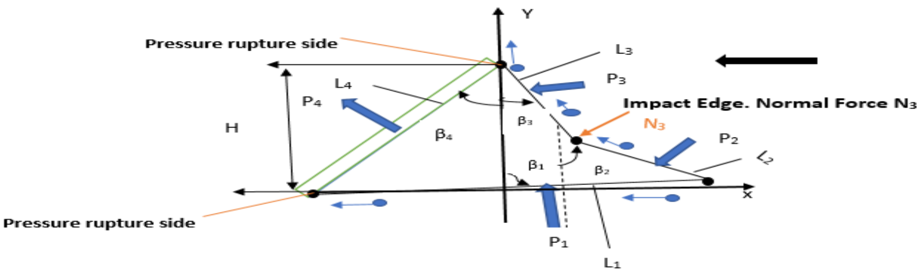

Fig. 3.6. Model of concave star-like prism form.
L_1, L_2, L_3, L_4 – length of sides; β₁, β₂, β₃, β₄ – frontal angles; H – height of prism.

[7] http://www.tf.llu.lv/conference/proceedings2020/Papers/TF170.pdf

3.4.3. 3D Numerical Computiations

A comparison of computation and theoretical interaction force (drag force) for diffferent prims is shown in Fig. 3.7, and ANSYS results are shown in Fig. 3.8.

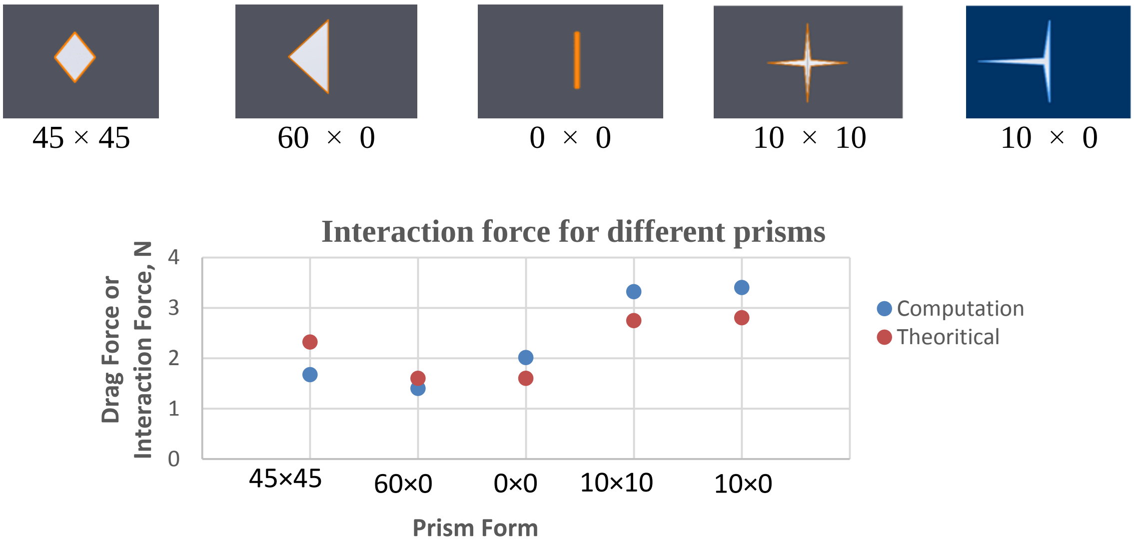

Fig. 3.7. Interaction force for different prisms comparison – numerical computation and theoretical approach.

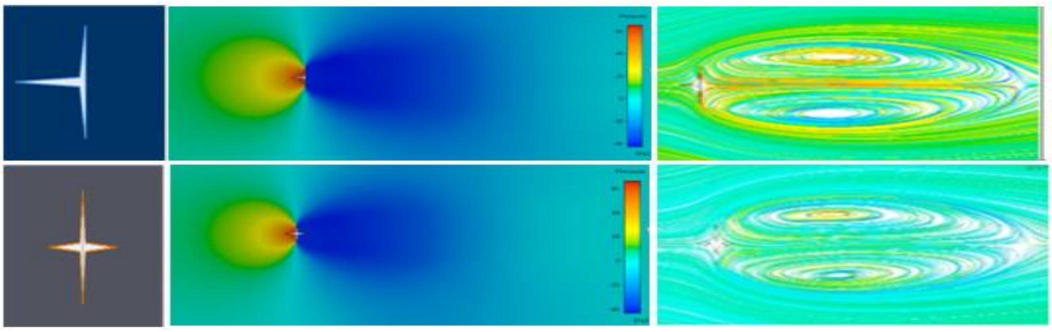

Fig. 3.8. Shape, pressure contour, streamlines for different star forms (10 × 10), (10 × 0).

3.5. Robotic Fish Tail with Fluid Interaction for Diving Motion

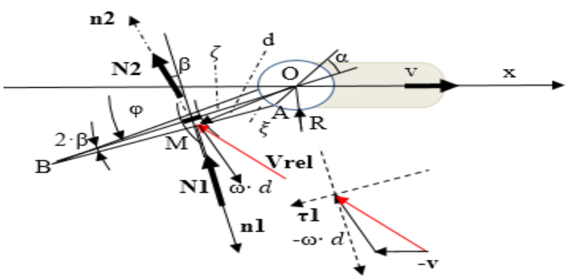

Fig. 3.9. Tail-fluid inteaction in diving motion for autonomous robotic.

Assuming a simple linear motion for the robotic fish in water with a mechatronic system, hull and the tail is described as a mechanical system of one degree of freedom (1DOF) defined by coordinate x. The differential equation for robotic motion is given in publication No. 1[8].

$$(m_0 + m)\ddot{x} = -N_1 x - N_2 x - b\dot{x}^2 \text{sign}(\dot{x}), \tag{33}$$

where m_0 is a mass of the hull; m is a mass of the tail; $\ddot{x}$, $\dot{x}$ are correspondingly the acceleration and velocity of the hull; $N_1 x$ is a fluid interaction component in a pressing zone; $N_2 x$ is a fluid interaction component with the tail in suction zone; $b\dot{x}^2$ is non-linear interaction of the hull with fluid in rectilinear motion, depending of motion velocity $v = \dot{x}$ directions; b is constant.

Forces N_{1x} and N_{2x} can be expressed as through interaction phenomenon:

$$F_1 x = |N_1| \text{sign}\left(v\sin(\varphi - \beta) + \omega \frac{R + R2}{2}\right) \sin(\varphi - \beta); \tag{34}$$

$$F_2 x = |N_2| \text{sign}\left(v\sin(\varphi) + \omega \frac{R + R2}{2}\right) \sin(\varphi) \tag{35}$$

All numerical results obtained from MATHCAD are shown in Figs. 3.10–3.13.

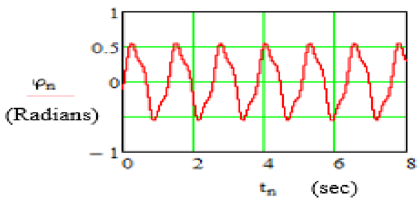

Fig. 3.10. Tail rotation angle with time.

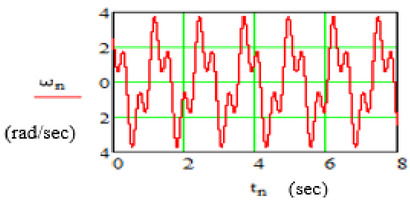

Fig. 3.11. Angular velocity with time for the robotic tail fin, $\lambda_3 = -0.1$.

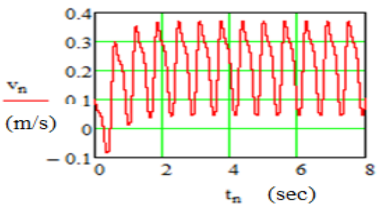

Fig. 3.12. Robotic fish hull velocity; $\lambda_3 = -0.1$.

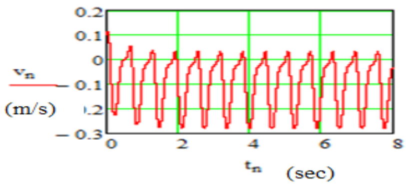

Fig. 3.13. Robotic fish hull velocity in reverse direction for $\lambda_3 = +0.1$.

3.6. Motion of Sharp Prism in Vertical Plane (Flying Object)

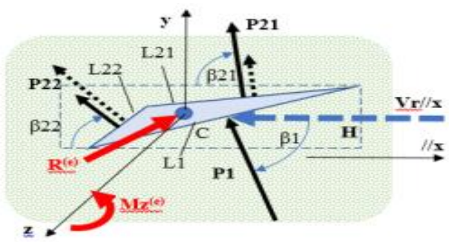

Fig. 3.14. Triangle prism movement along the wind direction.

8 https://dspace.emu.ee/xmlui/handle/10492/6054

For equal angles of $\beta_{22} = \beta_{21} = \beta_1$ in Fig. 3.14, a case of vertical movement is studied. The motion of a sharpened prism in a vertical plane is described by differential equations (36), (37). The obtained equations allow solving analytical and parametric optimization problems for a given non-stationary motion case.

$$m\ddot{x} = -[\rho LB(\dot{x}\sin(\alpha) - \dot{y}\cos(\alpha)^2 (1 + C_1)\sin(\alpha)\mathrm{sign}(\dot{x}\sin(\alpha) - \dot{y}\cos(\alpha)\sin(\alpha)], \quad (36)$$

$$m\ddot{y} = [LB\rho(\dot{x}\sin(\alpha) - \dot{y}\cos(\alpha)^2 (1 + C_1)\sin(\alpha)\,\mathrm{sign}(\dot{x}\sin(\alpha) - \dot{y}\cos(\alpha)^2] - mg, \quad (37)$$

where $\ddot{x}$ and $\ddot{y}$ are acceleration projections; α is angle between normal and vertical direction; sign is $a \pm 1$, depending of function in brackets; g is acceleration due to gravity.

Results of diving motion calculation are shown in Figs. 3.15–3.16. All parameters in system SI: $\rho = 1.25$; $LB = 0.04$; $mg = 2$; $C_1 = 0.5$; $\alpha = \frac{\pi}{4}$.

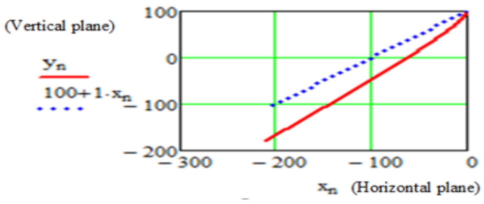

Fig. 3.15. The trajectory of the center of mass in the vertical plane from coordinates (x; y) = (0; +100).

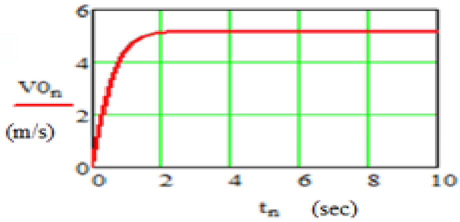

Fig. 3.16. Speed projection with varying time on prism normal.

4. PARAMETRIC AND CONTROL OPTIMIZATION FOR FLUID-RIGID BODY INTERACTION PROBLEM

4.1. Parametric Optimization of Star Prism

In the parametric optimization problem, the horizontal force F_x (as a criterion) is analyzed with equal sides $L_2 = L_3$ for the star prism with height H = constant and $\beta_1 = 0$ for different C_{12}, C_{23} value, Fig. 4.1. The example demonstrates that analytical relationships are obtained, which allow for parametric optimization of fluid flow interactions.

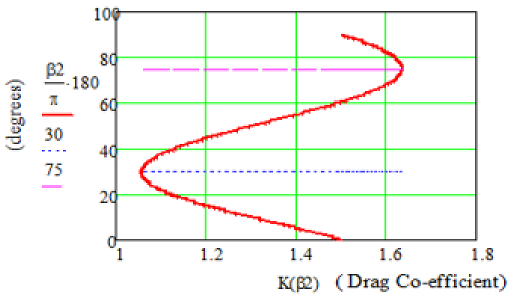

Fig. 4.1. Star prism (four sided) optimization result for the first criterion: $K(\beta_2)$ – drag coefficient; $C_{12} = C_{23} = 1$.

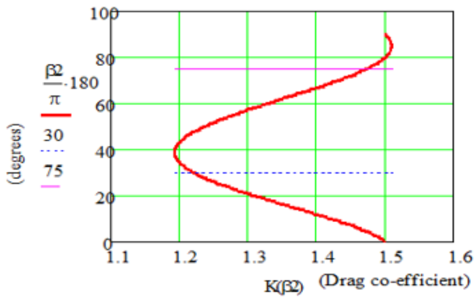

Fig. 4.2. Star prism (four sided) optimization result for the second criterion: $K(\beta_2)$ – drag coefficient; $C_{12} = C_{23} = 0.5$.

4.2. Energy Recovery from Fluid Flow

4.2.1. Energy Recovery Using Perforated Plate in Fluid Flow

The technique of energy extraction using a perforated flat plate that could switch between a simple plate and a perforated plate by means of efficient mechatronic system is demonstrated using a mathematical model. The mean value of the perforated plate investigated here is within the limits $-\frac{\pi}{4} \leq \beta \leq \frac{\pi}{4}$. The obtained constant C is 0.065. The mathematical model for the energy extraction concept is given by (38) taking into consideration the plate relative velocity, the plate is assumed to have negligible thickness ($d \cong 0$).

$$m\ddot{x} = -cx - b\dot{x} - A_0[1 - a\operatorname{sign}(\dot{x})]\rho\{C + [\cos(\beta_0)]^2]\}(V + \dot{x})^2 \frac{V + \dot{x}}{|V + \dot{x}|}, \tag{38}$$

where m, $x, \dot{x}, \ddot{x}$ is mass, displacement, velocity and acceleration of plate respectively; A_0 is middle value of interaction area parameter; a is the constant of area exchange; ρ is air density; C is vacuum constant; β_0 is the plate angle; V is air flow absolute velocity; $a\operatorname{sign}(\dot{x})$ is adaptive control area action. Modelling results are shown in Figs. 4.3–4.4.

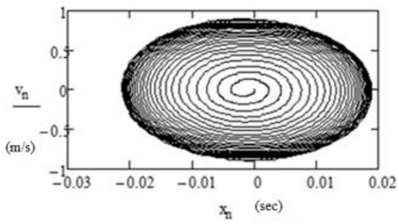

Fig. 4.3. Motion in phase plane.

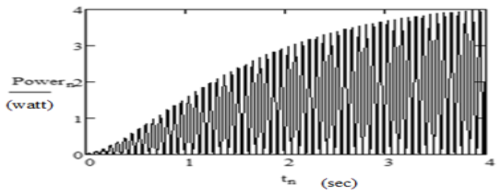

Fig. 4.4. Generator's power.

4.2.2. Energy from Diamond or Flat Plate

The thin plate (d ~ 0) model includes a linear spring with stiffness c and linear damping with proportionality coefficient b. According to the approximation theory, taken into account relative interaction velocity V_r, the differential equation of plate motion along the flow direction will be (39)

$$m\ddot{x} = -cx - b\dot{x} - A\rho[0.5 + \cos(\beta)^2](v_f + v_p)^2 \frac{(v_f + v_p)}{|(v_f + v_p)|} \tag{39}$$

where A is surface area of the plate; ρ is density; β is the plate angle against flow; v_f is fluid velocity; v_p is plate velocity along the flow direction. For $\beta = \frac{\pi}{2.5}\sin(7t)$, the modelling results are for A = 0.004 m^2; V = 10 m/s; ρ = 1,25 kg/m^3 are shown in Figs 4.5–4.6.

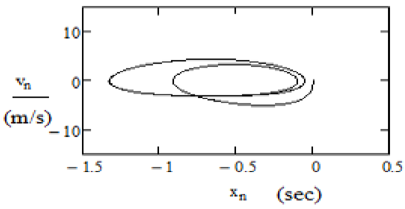

Fig. 4.5. Motion in phase plane.

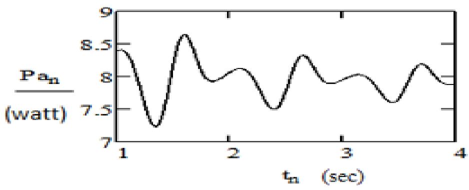

Fig. 4.6. Average power of generator force.

4.2.3. Energy Recovery from a Dual Varying Area Actuator of a Robotic Fish

Only during the diving motion the tail form is changed from single to dual tail that could rotate about axis O as shown in Figs. 4.7–4.8.

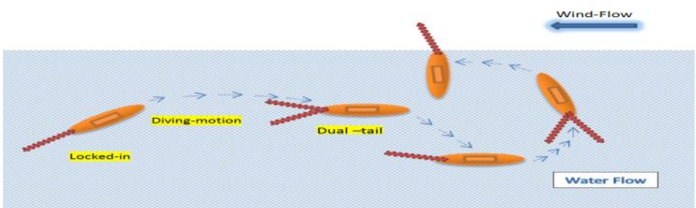

Fig. 4.7. Flapping actuator in diving motion for dual tail and single tail fin inside water along with the technique of charging from air.

From 4.8, taking the air interaction

$$J_z\ddot{\varphi} = Mwin_z - Mel_z(\varphi) - Mgen_z(\dot{\varphi}), \tag{40}$$

where J_z is a tail mass moment of inertia about rotation axis z; $\ddot{\varphi}$ is angular acceleration; $\varphi, \dot{\varphi}$ are correspondingly the angle and angular velocity; $Mwin_z$ is an air flow interaction moment; $Mel_z(\varphi)$ is a moment from linear or non-linear elastic spring; $Mgen_z(\dot{\varphi})$ is a linear or non-linear moment from energy generator.

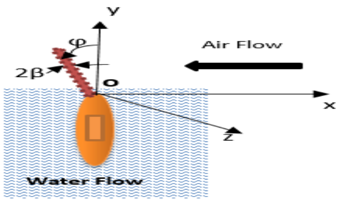

Fig. 4.8. Charging action (projecting the tail out of water surface).

The results of the mathematical modelling are given for a relatively small plate. A case with a linear spring and a linear generator characterization in the following form is considered:

$$Mel_z = c\varphi;\ Mgen_z(\dot{x}) = b\dot{\varphi}, \tag{41}$$

where c, b are the constants.

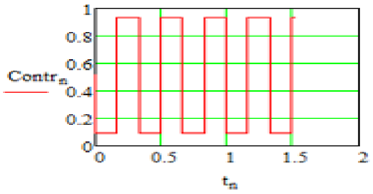

Fig. 4.9. Area control action.

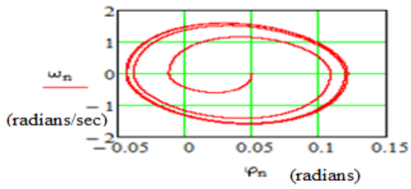

Fig. 4.10. Motion in phase plane.

4.2.4. Energy Recovery Using Single Actuator for Robotic Fish

Wind flow interaction is given by (42) (Publication No. 7[9]), and the results are illustrated in Figs. 4.11–4.12:

$$Q = B \cdot L \cdot MCP \cdot \rho(1 + C)[V \sin(\alpha) - \omega r \cos(\alpha - \varphi)]^2 \cdot \operatorname{sign}[V \sin(\alpha) - \omega r \cos(\alpha - \varphi)], \tag{42}$$

where MCP is the function of area Mechatronics Control of Perforated plate; ρ is density; V is wind velocity; α is the plate angle with respect to the wind (fluid flow); r is the length of rods; φ is the angle of rods; ω is angular velocity; C is constant at the suction zone.

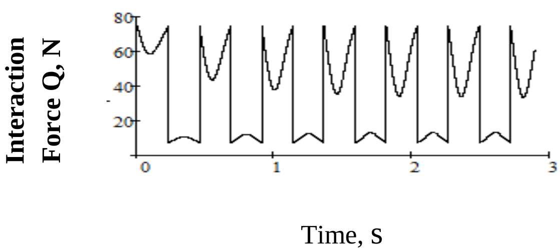

Fig. 4.11. Wind flow interaction forces Q as a function of time t.

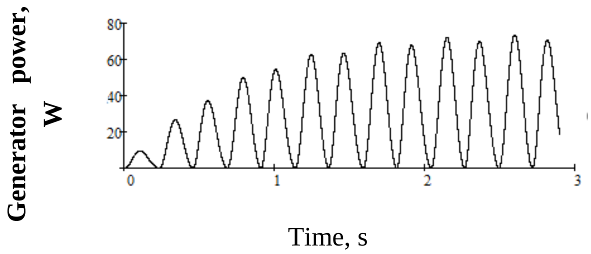

Fig. 4.12. Instantaneous generator power.

[9] https://link.springer.com/chapter/10.1007%2F978-981-15-8025-3_72

4.3. Vibration Damping from Fluid Interaction through Parametric Optimization

4.3.1. 1DOF System Free Vibration Damping from Impacts and Interactions

A case of impact and interactions is analyzed in this section for a wheel hitting an elevated surface. The area of the body under consideration is analysed for water medium, for it was understood that to generate the same power, the area is to be increased many times. Neglecting the viscous nature of the medium, the equations as per the laws of classical mechanics are obtained and the results are given in Figs. 4.13–4.14.

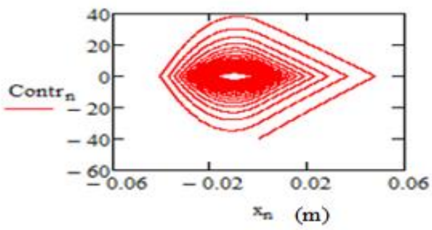

Fig. 4.13. Control action vs displacement.

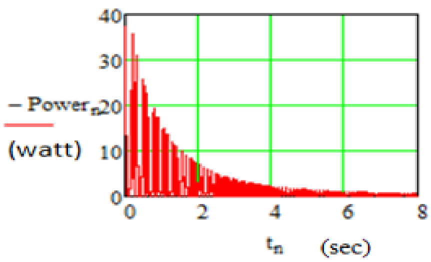

Fig. 4.14. Power generated with varying time.

4.3.2. 1DOF System (Linear and Non-Linear Spring) Free Vibration Damping Subjected to Harmonic Excitation

(a) A resonance case for linear- and non-linear spring is taken up in different fluid medium as is subjected to a harmonic excitation. Linear-spring, resonance $\omega = \sqrt{\dfrac{c}{m}}$ for water as fluid medium. The results of which are shown in Figs 4.15–4.16.

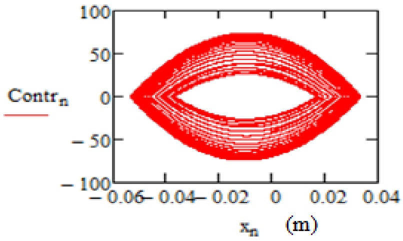

Fig. 4.15. Control action with varying time.

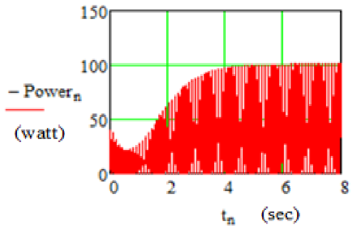

Fig. 4.16. Power generated as a fuction of time.

(b) Non-linear spring, cubic elasticity: cx^3. Resonance $\omega = \dfrac{1}{3}\sqrt{\dfrac{c}{m}}$, gas as fluid. The results are illustrated in Figs. 4.17–4.18.

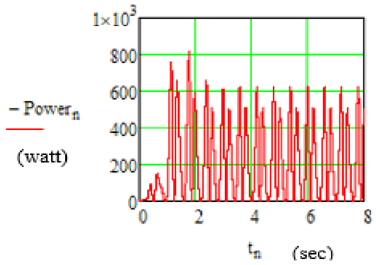

Fig. 4.17. Power generated for water.

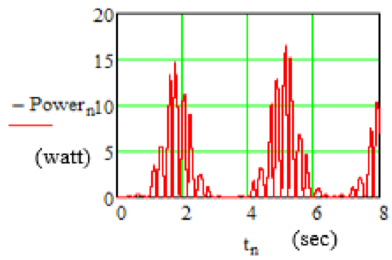

Fig. 4.18. Power generated for gas (air).

4.3.3. 1DOF System Damping for Harmonic Excitations in Water, Non-Periodic Case

The transition process from zero to excitation force frequency was analyzed. The results of which are shown in Figs. 4.19 and 4.20.

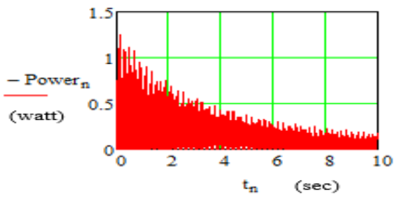

Fig. 4.19. Power generated for water as working medium with varying time.

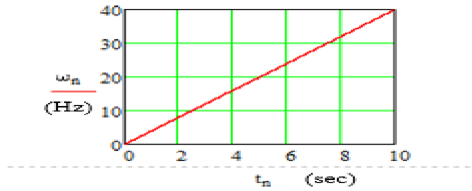

Fig. 4.20. Linear trend of frequency with varying time.

4.4. Control Optimization of Fluid Interaction

4.4.1. Simple Horizontal Motion Model Optimization with Force Control

From the **Pontryagin's maximum principle** for the simple horizontal motion with force control for a robotic fish, we have the solution for optimal control, where P_0 is maximum power force 1) if (exponent) > 0, $P = P_0$; 2) if (exponent) < 0, $P = 0$.

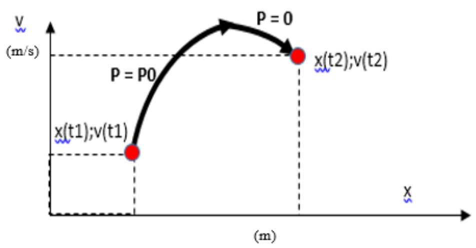

Fig. 4.21. Optimal control in phase plane (x; v_0).

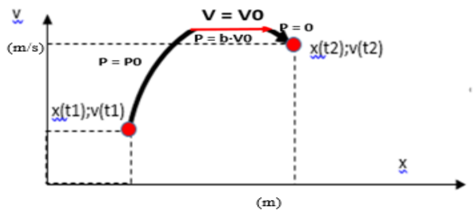

Fig. 4.22. Optimal control in phase plane (x; v_0) with limit of velocity ($v < V_0$).

4.4.2. Simple Vertical Motion Model with Force Control

The main difference here is that all-time control is complemented by two forces: gravity force mg and Archimedes force A. Since they are constant, the optimal control is similar to the horizontal case. However, the difference is that swimming or sinking rules must be taken into account. If the robot has a neutral buoyancy ($A = mg$), the control corresponds exactly to the horizontal control case.

4.4.3. Optimization of Shape (Form) of Flow Interaction Surface

The optimization problem is solved in three tasks.

Task 1. It should be noted that the form could be searched for as a polynomial.

Task 2. Model of two opposite curved planes.

Task 3. Model of two **concave** planes.

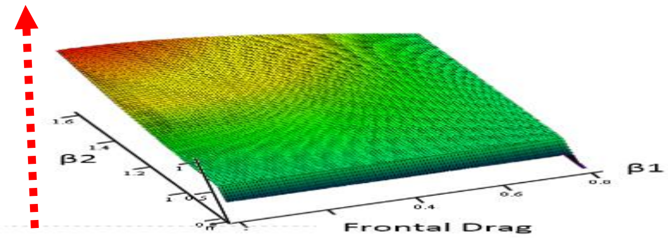

Fig. 4.34. Maximum and minimum force F solution graph: **maximum** force *F* is at $\beta_1 = 0$; $\beta_2 = \pi/2$ (90°). The minimum force is at $\beta_1 = \beta_2 = \pi/4$ (45°).

5. SYNTHESIS AND MOTION MODELLING OF NEW ENERGY SCAVENGING SYSTEMS

5.1. Single Degree of Freedom System (with Varying Area Prism)

A new complex system (electro-mechanical system) is synthesized using the phenomenon of fluid-rigid body interaction. The energy is obtained by an electro-dynamic braking system 4, Fig. 5.1. The differential equation of motion is (43):

$$m\ddot{x} = -f(x) - D(\dot{x}) - A\rho[V_0\cos(\beta-\alpha) + \dot{x}\cdot\cos(\beta)^2] \cdot \mathrm{sign}[V_0\cos(\beta-\alpha) + \dot{x}\cos(\beta)^2] \tag{43}$$

where $f(x)$ is spring characteristic; $D(\dot{x})$ is force of electro-dynamic braking system; A is prism area of pressing zone, as before: $A = LB$.

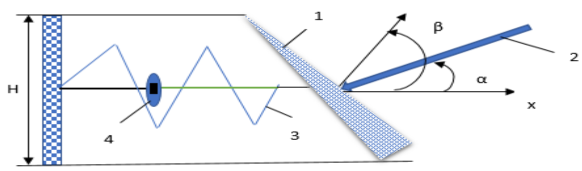

Fig. 5.1. Model for energy extraction using phenomenon of air-body (prism) interaction: 1 – sharp triangular prism; 2 – wind flow; 3 – elastic spring; and 4 – electro-dynamic braking system.

Solving (43) is for all kinds of analytical, optimization and synthesis problems if a criterion with given constraints on system and control parameters is formulated. When taking into account the case of linear spring with a linear electrodynamic braking system, equation (43) is expressed as (44):

$$m\ddot{x} = -cx - b(\dot{x})\dot{x} - A(\dot{x},x,t)\rho(V_0\cos(\beta-\alpha) + \dot{x}\cos(\beta)^2) \cdot \mathrm{sign}(V_0\cos(\beta-\alpha) + \dot{x}\cos(\beta)^2), \tag{44}$$

where c is elasticity of spring; $b(\dot{x})$ is electrodynamic systems control force; $A(\dot{x},x,t)$ is area variation control action, depending on synthesis task of velocity, coordinate and time.

We consider the possibility of obtaining energy from the flow if the change of area occurs instantaneously when opening or closing the perforation. We assume the simplest direction of the wind flow parallel to the prism motion axis $\alpha = 0$ and with optimal angle $\beta = 0$ (Fig. 5.1). Then the differential equation of motion is to be given by (45):

$$m\ddot{x} = -cx - b(\dot{x}) - (1 + C_1)A[a_0 - a_1\mathrm{sign}(\dot{x}\Delta v)]\rho(V_0 + \dot{x})^2 \cdot \mathrm{sign}(-V_0 - \dot{x}), \tag{45}$$

where b, C_1, a_0, a_1, Δv are constants. For parameters: $m = 0.5$ kg; $c = 80$ kg/s^2; $b = 0.5$ kg/s; $C_1 = 0.5$; $A = 0.04$ m^2; $a_0 = 0.75$; $a_1 = 0.25$; $\Delta v = 0.5$ m/s; $\rho = 1.25$ kg/m^3; $V_0 = 10$ m/s the modelling results are shown in Fig. 5.2–5.3.

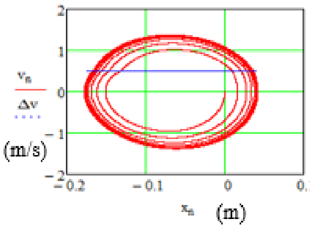

Fig. 5.2. Motion in phase plane.

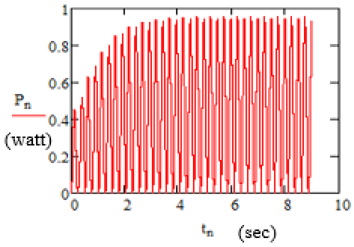

Fig. 5.3. Power generated.

5.2. Two Degrees of Freedom System (Using Rotating Perforated Plate)

A new electro-mechanical system is synthesized using a flat circular plate with alternate perforated quadrants in fluid flow as shown in Fig. 5.4. Motion analysis in a 2D space is shown in Figs. 5.5–5.7. The system considered consists of the two concentric circular plates fixed at the center, the plate whose front area is subject to fluid flow is to rotate freely over the other circular plate (non-rotating), both plates have the same area and alternate perforated quadrants, the spring, the linear generator in an incoming flow with a velocity V_0 (10m/s).

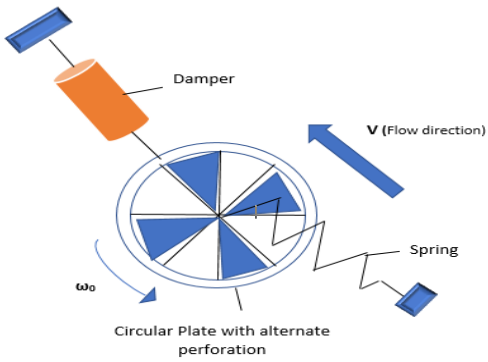

Fig. 5.4. Flat circular plate with alternate perforated quadrants.

$$Control = 1 + \frac{\arccos[\cos(\omega_0 t)]}{\pi}$$

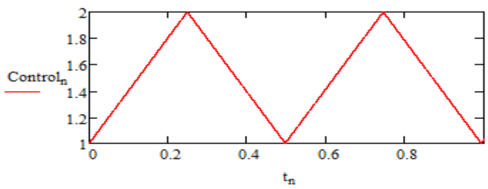

Fig. 5.5. Area control action: t – time.

Differential equation of circular plate motion (Fig. 5.5) is given by (46):

$$m\ddot{x} = -cx - \left[F_0 \operatorname{sign}(\dot{x}) - b\dot{x}\right] + \\ + (1+C)\frac{A}{\pi}\left\{\operatorname{acos}\left[\cos(\omega_0 t)\right] + \pi\right\}\rho(-V_0 - \dot{x})^2 \operatorname{sign}(-V_0 - \dot{x}), \quad (46)$$

where m is mass; x is displacement; $\dot{x}$ is velocity; c is stiffness of linear spring; F_0, b are constants of linear generator damping; (1 + C) is coefficient of interactions; V_0 is flow velocity; ω_0 is control actions harmonic angular frequency; A is constant area; ρ is air density.

The task of parametric optimization is as follows: to find a combination within the seven-parameter (m, c, F_0, b, ω_0, A, V_0) space with given constraints on the parameter values that provide the maximum power generated by the flow. The best combination of the three parameters (m, c, ω_0) is close to the resonance zone: $\omega_0 = \sqrt{\dfrac{c}{m}}$. The graphs for this case are shown in Figs. 5.6–5.7.

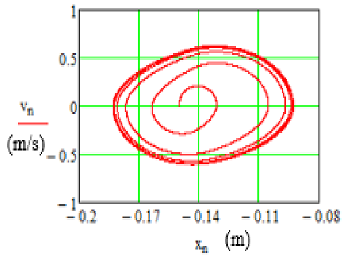

Fig. 5.6. Motion in phase plane.

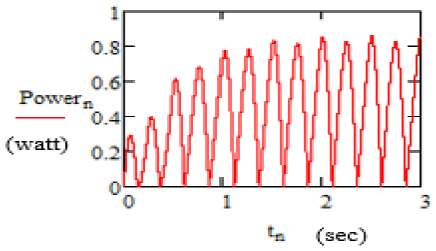

Fig. 5.7. Small plate power.

5.3. Three Degrees of Freedom System

A new device – flutter of axially streched flat ribbon model is synthesized. The axially stretched ribbon model is simplified to a system of three degrees of freedom (Fig. 5.8).

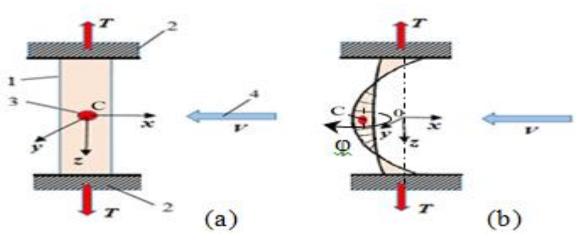

Fig. 5.8. Model of straight flat ribbon for (a) initial condition, deformed state.

According to the given 3DOF model of motion, the expression of the relative velocity of a local point in vector form is as follows:

$$V_{\xi,\mathrm{n}} = \left\{ \begin{pmatrix} -(V + \dot{x}\cos(\varphi) - \dot{y}\sin(\varphi) \\ (V + \dot{x}\sin(\varphi) - \dot{y}\cos(\varphi) - \xi\omega) \end{pmatrix} \right\} \cdot \begin{Bmatrix} i \\ j \end{Bmatrix} \tag{47}$$

Using (47) we can find the normal components of the flow interaction N_{f} and moment M_{f} as follows:

$$N_{\mathrm{f}} = (1 + C)B\rho \left\{ \int_{-h}^{h} [V + \dot{x}\sin(\varphi) - \dot{y}\cos(\varphi) - \xi\omega]^2 \right\} \xi d\xi; \tag{48}$$

$$M_z\left(P_{f(x,y)}\right) = (1 + C)B\rho \left\{ \int_{-h}^{h} [(V + \dot{x}\sin(\varphi) - \dot{y}\cos(\varphi) - \xi\omega]^2 \right\} \xi\varepsilon d\xi; \tag{49}$$

$$\varepsilon = \mathrm{sign}[V + \dot{x}\sin(\varphi) - \dot{y}\cos(\varphi) - \xi\omega], \tag{50}$$

where C is a constant, for example 0.5; B is a width of the plate; ρ is an air density; h is a half of plate height. Numerical results are in MATHCAD.

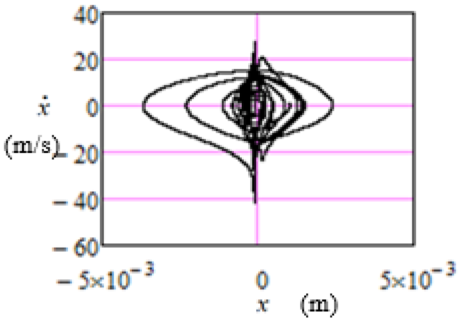

Fig. 5.9. Centre of mass motion in phase plane $(x;\dot{x})$.

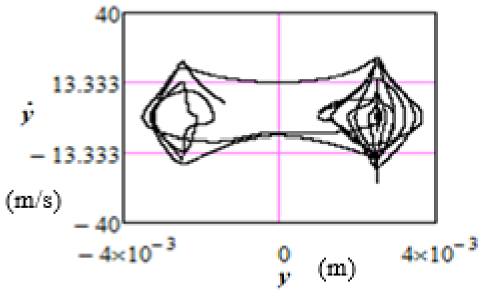

Fig. 5.10. Centre of mass motion in phase plane $(y;\dot{y})$.

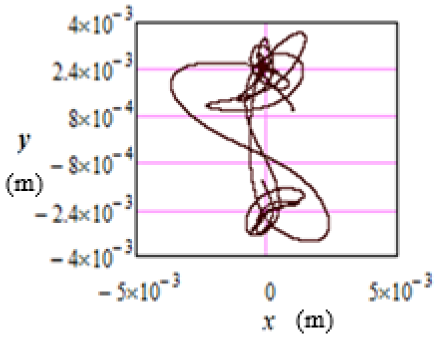

Fig. 5.11. Centre of mass motion in vertical plane (x; y).

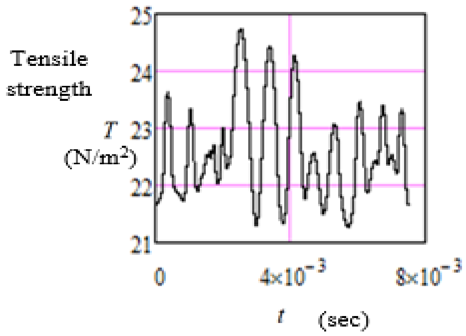

Fig. 5.12. Total tensile strength T of the elastic elements, depending on the time.

6. EXPERIMENTAL INVESTIGATIONS

Experiments were carried out in the arm field wind tunnel available at Riga Technical University. Initially, experiments for the square flat plate were performed at a constant uniform speed of 10 m/s in the wind tunnel. The edge length of the flat plate was taken to be 0.16 m and the similar square flat plate with perforations (the area of perforations maintained at half the area of the plate) is experimented (Fig 6.1). The drag force is measured using the concepts of balanced weights. Figure 6.2 shows a perforated plate experiment at different angles to flow for measuring interaction force, drag.

6.1. Perforated Plate Experiment in Wind Tunnel

Experiments for different alignment of perforations were also carried out (horizontal and vertical), as shown in Fig. 6.2.

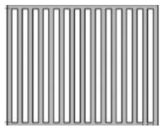

Fig. 6.1. Perforated plate with perforations aligned vertically.

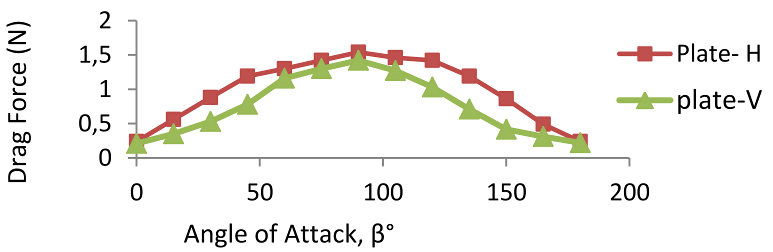

Fig. 6.2. Experiments for perforated plate, perforations aligned in horizontal and vertical at a wind speed of 10m/s.

Simple form objects

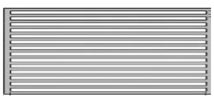

Perforated plate

Triangular prism

Flat triangular prism

Flat plate

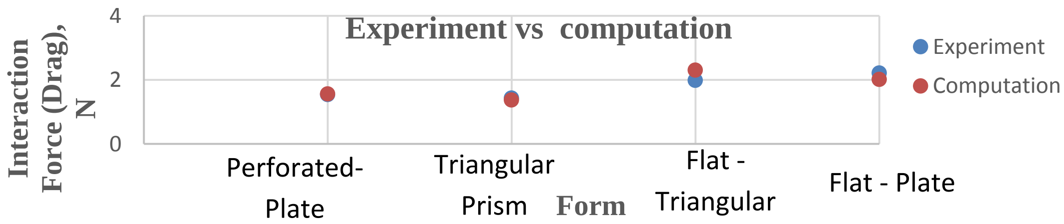

Fig. 6.3. Experiments and computation interaction force results for different forms at a constant speed of 10 m/s.

6.2. Inspection of a New Flapping/Oscillating Device

A new oscillating/flapping device that is fully 3D printed (Fig. 6.5) is experimented at different speeds. From the experiments the fact is that with flow induced vibration by inserting the plate downstream of a cylinder would not help obtain energy, the same is true with the perforated plate. Therefore, in the suction area with a plate, the vortices are inefficient and cannot be used for energy scavenging.

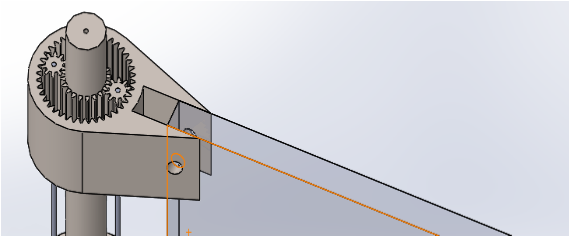

Fig. 6.4. 3D design of model from solid works.

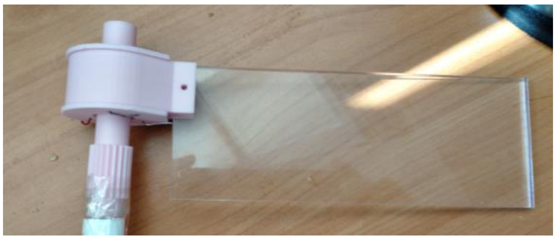

Fig. 6.5. Prototype of the flapping device.

6.3. Validation of Theory with Experiments

6.3.1. Damping Oscillations of Thin Plates in the Open Air in Rotational Movement

For the purpose of testing the theory, experiments in the open air with decreasing oscillations of thin plates in rotational movement is performed. A simple experiment-setup to validate the theory of interaction coefficient *C* taking the concept of zones (pressure and suction side) is performed. It was noted that in reality the difference between the theory and experiments was only about 1.8 %. The experiment setup is shown in Fig. 6.6.

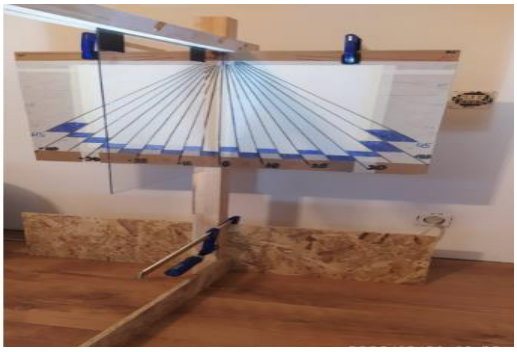

Fig. 6.6. Motion of pendulum oscillating (experimental setup).

6.3.2. Comparison of Theory and Experiment for *C* (0.5)

Differential equation of physical motion pendulum is given by:

$$\ddot{\varphi} = -3\,g\left(\frac{1}{2}\right)\sin(\varphi) - (1+C)B\rho\left[\frac{3L^2}{4m}(\dot{\varphi})^2\right]\operatorname{sign}(\dot{\varphi}), \tag{51}$$

where φ is the angular diaplcement; *L* is length; m is mass; *C* is coefficient of interaction; *B* is depth of the pendulum.

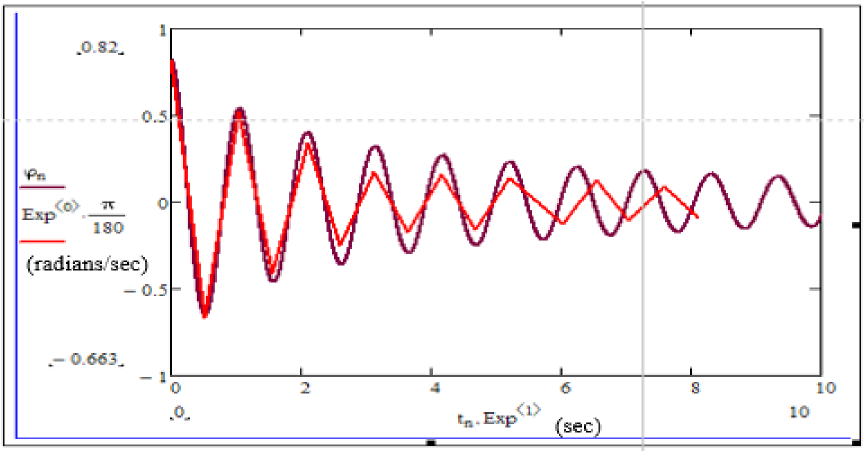

Fig. 6.7. Angular displacement with time (comparison of experiment and numerical calculation).

6.3.3. Comparison of Theory and Experiment for *C* (0.25)

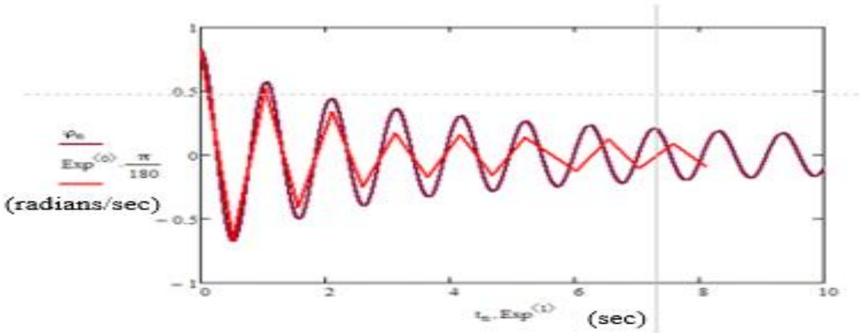

Fig. 6.8. Angular displacement with time for *C* = 0.25 (comaprison of experiment and numerical calculation).

6.4. New Invention

A new patent application was submitted on the topic “Wind energy conversion device” by Riga Technical University, application No. LVP2020000092.

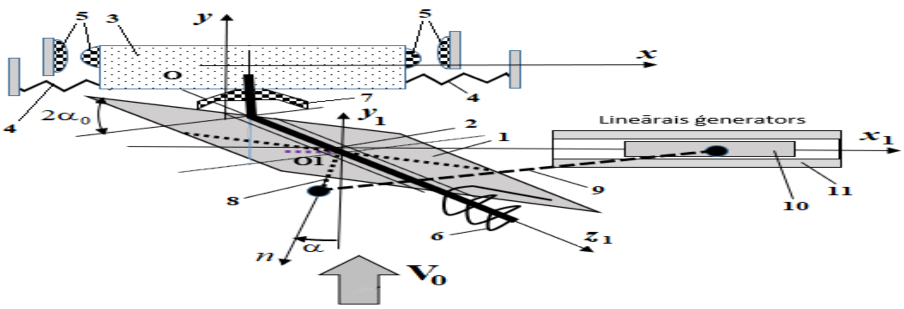

Fig. 6.9. Schematic representation of energy scavenging using flapping/oscillating plate in air flow.

The wind energy conversion device contains a flat blade (1) (Patent publication No. 9[10]) attached to the rotating axle (2) by a cylindrical axial pivot, symmetry axis z_1 of the flat blade (1) and is firmly connected to the slider (3), the translation movement (3) is limited by springs (4) and shock absorbers (5). The blade turning (1) around (2) is limited by the rotational spring (6) and rotational shock absorber (7). Perpendicular to the lateral surface (1), a crank (8) is firmly attached, which is connected by a pivot to the connecting rod (9) which, in turn, is connected by a pivot to the slider (10) of a linear generator, which has the ability to move along the inside of the electric coil (11) in the direction of the x_1 axis.

The invention relates to wind energy, mainly to wind turbines which convert the kinetic energy of the wind flow into other forms of energy (for example, the kinetic energy of the actuator of the machine, or the potential energy of the air compression compressor, or the electrical energy stored in a special device). The object of the invention is to increase the operational safety of a wind energy conversion plant and the efficiency of a wind energy plant. The wind energy conversion device comprises a flat blade (1) attached to a rotating shaft (2) with a cylindrical axial joint. The longitudinal axis of the rotating axis (2) coincides with the symmetry axis z_1 of the flat blade (1) and is firmly connected to a slider (3) which has the ability to move along special guides in the x-axis direction, the slider (3) being limited by springs (4) and shock absorbers (5). In turn, the rotation of the flat blade (1) around the rotating axis (2) is limited by the rotational spring (6) and the rotational damper (7). A crank (8) is firmly attached to the side surface of the flat blade (1) and is hinged to the connecting rod (9). In turn, the connecting rod (9) is hinged to the linear generator slider (10), which can move along the inside of the electric coil (11) in the direction of the x_1 axis.

[10] http://www.tf.llu.lv/conference/proceedings2021/Papers/TF213.pdf
[11] Patent application No. LVP2020000092. R.T.U., 18-12-2020.

GENERAL CONCLUSIONS

1. In the present work, only air as a surrounding medium is taken into consideration but the technique with minor variations can be extended for other fluids of interest where rigid body-fluid interactions are to be studied. The fluid medium should be continuous (continum).
2. The task of optimization as discussed can also be extended for complex geometries, but only at low speeds.
3. For synthesis of new mechanical systems, object parameters play an important role along with the interaction phenomenon.
4. In the present work, a linear damper is deployed. It is anticipated that a different type of damper (non-linear damper) would increase the efficiency of the overall system under consideration.
5. The importance of coefficient of interaction C is well discussed and best used for the tasks of energy scavenging, synthesis and optimization through fluid-rigid body interaction phenomenon. Though viscous nature of the fluid medium is not considered, the interaction coefficient C as an alternative, good results could be achieved.
6. Parametric optimization is needed if a very good efficiency is desired.
7. In the case of unsteady flow, the constant pressure at the boundary layer just downstream of the object gets split at the point of symmetry. Thus, there can be seen a variation in pressure on the either side of the symmetry in the leeward (downstream) side.
8. The results are only valid for a rigid body and fluid interaction at low speeds.
9. The concept or technique proposed in the work is first of its kind that helps eliminate complex ‘space-time’ programming techniques and is an advantage to analyse the phenomenon of non-stationary motion in a fluid flow.
10. When considering the interaction phenomenon for a rigid body in air, the viscosity of the medium (air) is of secondary importance. The object parameters, selection of type of damper, form or shape of the object subjected to the fluid flow and nature of flow laminar or turbulent are of primary importance.